

# Design, theory, and measurement of a polarization insensitive absorber for terahertz imaging

N. I. Landy<sup>1</sup>, C. M. Bingham<sup>1</sup>, T. Tyler<sup>2</sup>, N. Jokerst<sup>2</sup>, D. R. Smith, and W. J. Padilla<sup>1</sup>  
<sup>1</sup>*Boston College, Department of Physics, 140 Commonwealth Ave., Chestnut Hill, MA 02467. and*  
<sup>2</sup>*Department of Electrical and Computer Engineering, Duke University, Durham, NC 27708 USA.*

We present the theory, design, and realization of a polarization-insensitive metamaterial absorber for terahertz frequencies. We derive geometrical-independent conditions for effective medium absorbers in general, and for resonant metamaterials specifically. Our fabricated design reaches and absorptivity of 65% at 1.145 THz.

## INTRODUCTION

The advent of terahertz (THz) spectroscopy has ushered in a new field of research as scientists seek to exploit the electromagnetic signatures of materials in the THz range of the spectrum. Specifically, the ability to perform imaging in the THz would have profound impact on the areas of security[1, 2, 3, 4], biology[5, 6], and chemistry[7, 8]. However, imaging in the terahertz is complicated by the a lack of easily accessible electromagnetic responses from naturally occurring materials. [9, 10]

Electromagnetic metamaterials (MMs)[11, 12] are one potential solution to overcoming this “THz Gap”[13]. The operational frequency of a given MM design is geometrically scalable to other regimes of the electromagnetic spectrum. Various MM structures have been shown to naturally couple to either the electric and / or magnetic components of light in frequency ranges from radio [14], microwave [15], mm-Wave [16], THz [13], MIR [17], NIR [18], to the near optical [19]. A great deal of effort has been exerted to create low-loss metamaterial devices such as negative index (NI) structures [15] and electromagnetic cloaks[20, 21]. However, the substantial loss tangent that occurs at the center frequencies of metamaterial resonances can be exploited as well. This resonant loss phenomenon serves as the starting point for the investigation of MMs as narrow-band absorbing elements for thermal imaging devices.

We present the theory, design, fabrication, and measurement of a single-frequency metamaterial absorbing element. The simulated design reaches a peak absorptivity of 95% at 1.13 THz and the fabricated structure reaches a measured absorptivity of 65% at 1.145 THz. This absorptivity is comparable to existing MM absorber designs [22, 23], but our design is also polarization insensitive, which maximizes the absorption of light.

## THEORY

The absorptivity  $A(\omega)$  of a given material is given by the transmission  $T(\omega)$  and reflectance  $R(\omega)$  as  $A(\omega) = 1 - T(\omega) - R(\omega)$ . In terms of the complex transmis-

sivity ( $\tilde{t}$ ) and reflectivity ( $\tilde{r}$ ), this can be written as  $A = 1 - |\tilde{t}(\omega)|^2 - |\tilde{r}(\omega)|^2$ . Therefore,  $A = 1$  when  $T = R = 0$ . In reference [24], the frequency-dependent transmissivity  $\tilde{t}(\omega)$  was determined to be dependent on the complex index of refraction  $\tilde{n}(\omega) = n_1 + in_2$  and impedance  $\tilde{Z}(\omega) = Z_1 + iZ_2$  for a slab of length  $d$  as:

$$t(\omega)^{-1} = \sin(\tilde{n}kd) - \frac{i}{2} \left( \tilde{Z} + \frac{1}{\tilde{Z}} \right) \cos(\tilde{n}kd). \quad (1)$$

Where  $k = \omega/c$  and  $c$  is the speed of light in vacuum. We use the convention where a subscripted 1 and 2 denote the real and imaginary parts of a complex function, respectively.

As  $\tilde{Z}$  approaches unity (the free space value), the reflectivity will drop to zero and the transmissivity will be determined entirely by  $\tilde{n}$ :

$$t^{-1} = \cos(\tilde{n}kd) - i \sin(\tilde{n}kd). \quad (2)$$

Upon substitution of the exponential forms this becomes:

$$t^{-1} = e^{-in_1kd} e^{n_2kd}. \quad (3)$$

So the transmission ( $T = |\tilde{t}|^2$ ) is

$$T = e^{-2n_2kd}. \quad (4)$$

Therefore, as  $n_2$  approaches infinity,

$$\lim_{n_2 \rightarrow \infty} T = 0. \quad (5)$$

The combined dielectric and magnetic losses in the system are characterized by  $n_2$ . Therefore the physical interpretation of the above derivation is that, (in the absence of reflections), the transmission of an electromagnetic wave with a given wavevector  $k$  through a slab of given thickness  $d$  is determined entirely by losses in the slab. To create a very high absorber it is then necessary for  $\tilde{Z} = 1$  at a point where  $n_2$  is large.

Precise control of  $\tilde{n}$  and  $\tilde{Z}$  is necessary to realize a high absorber. Electromagnetic MMs are prime candidates for this task since they can be designed to couple to electric and magnetic components of light. This enables precise tuning of the complex, frequency-dependent permittivity  $\tilde{\epsilon}(\omega)$  and permeability  $\tilde{\mu}(\omega)$  of a MM slab. The index  $\tilde{n}$  and impedance  $\tilde{Z}$  are in turn given by  $\tilde{n}(\omega) = \sqrt{\tilde{\epsilon}(\omega)\tilde{\mu}(\omega)}$  and  $\tilde{Z}(\omega) = \sqrt{\tilde{\mu}(\omega)/\tilde{\epsilon}(\omega)}$ .

MMs are typically highly resonant in  $\tilde{\epsilon}$  and / or  $\tilde{\mu}$ , where the relevant optical constants approximate the form of a complex oscillator in frequency:

$$\epsilon(\omega), \mu(\omega) = \epsilon_{\infty}, \mu_{\infty} + \frac{F_{\epsilon, \mu} \omega^2}{\omega_{0\epsilon, \mu}^2 - \omega^2 - i\gamma\omega} \quad (6)$$

where  $F$  is the oscillator strength,  $\gamma$  is the damping,  $\omega_0$  is the center frequency of the oscillator, and  $\epsilon_{\infty}, \mu_{\infty}$  are high frequency contributions to  $\epsilon, \mu$ . This form for an oscillator describes the frequency response of metamaterials, and we term this a ‘‘Pendrian’’ after ref. [12].

We consider a single frequency operation point, defined by  $\omega_0$ , such that when  $\tilde{\epsilon}(\omega_0) = \tilde{\mu}(\omega_0)$  then  $\tilde{Z}(\omega_0) = 1$  and  $n_2(\omega_0)$  is maximized with a value of:

$$n_2(\omega_0) = \frac{F^2}{(\gamma\omega_0)^2} \quad (7)$$

which, according to Eq. 4, yields

$$A(\omega_0) = 1 - \text{Exp}\left(-2\frac{F\omega_0^2 d}{\gamma c}\right) \quad (8)$$

For the more realistic case, when  $\epsilon_{\infty} \neq \mu_{\infty}$ , then  $\tilde{Z}(\omega_0) = \sqrt{\mu_{\infty}/\epsilon_{\infty}} \neq 1$  and  $A$  is no longer determined solely by  $n_2$ . However, for large  $n_2$ ,  $T(\omega_0)$  remains low and  $R(\omega_0)$  can be written approximately in terms of  $Z(\omega)$  [24] such that

$$R(\omega_0) = \left(\frac{Z(\omega_0) - 1}{Z(\omega_0) + 1}\right)^2 \quad (9)$$

Regardless of  $\epsilon_{\infty}$  and  $\mu_{\infty}$ , an optimal narrow-band absorber must maximize  $F$  with respect to  $\gamma$  in both  $\epsilon$  and  $\mu$ .  $F$  is determined by the geometry, filling factor, and conductivity of the two metallizations.  $\gamma$  is determined by losses in the metallization and substrate. The optimal absorber will then use the MM geometries with the maximum possible filling factor. Furthermore, metallization and substrate should be chosen to minimize losses at the operation frequency as determined by Eq. 7 above.

## DESIGN

From a theoretical viewpoint, it would seem simple to design a MM that would provide such a response in

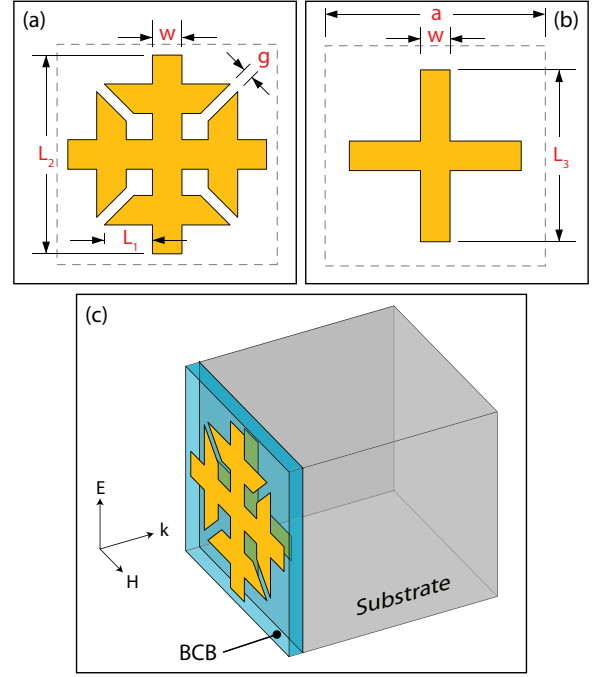


FIG. 1: (color) (a) ERR (b) cross (c) combined ERR and cross. The dimensions in microns are  $a = 84$ ,  $L_1 = 52.5$ ,  $L_2 = 74$ ,  $L_3 = 64$ ,  $w = 11$ , and  $g = 4$ . Axes indicate the wave polarization and propagation direction.

$\epsilon$  and  $\mu$ . However, there are several complications to the theoretical analysis presented above due to the specific properties of MMs. For instance, the periodicity inherent to most MMs contributes to spatial dispersion, i.e.  $\epsilon = \epsilon(\omega, \mathbf{k})$  and  $\mu = \mu(\omega, \mathbf{k})$ . [25] This spatial dispersion causes the optical parameters to deviate from the pure form of Eq. 6. Spatial dispersion also causes antiresonances in  $\tilde{\mu}$  ( $\tilde{\epsilon}$ ) due to resonances in  $\tilde{\epsilon}$  ( $\tilde{\mu}$ ) [26]. Additionally, conventional electric [27, 28] and magnetic [15] MMs are highly coupled when they share a center resonant frequency [29]. Typically, electric metamaterials have higher order electric resonances, and thus in general one does not necessarily have the condition that  $\epsilon_{\infty} = \mu_{\infty}$ , leading to a nonzero reflectivity as described above. In our particular case for the design of a narrow-band high absorber, a solution to the latter problem was to use two electric resonances; one to raise and lower the curve at the operational frequency and one to couple to  $\mu$  to create a region of high absorption.

The electric responses were provided by a modified electrically coupled ring resonator (ERR), shown schematically in Fig.1(a). The ERR chosen had four-fold rotational symmetry about the propagation axis and was therefore polarization insensitive [27]. The lower-frequency electric response used to tune the  $\epsilon(\omega)$  curve was driven by the LC loop in the ERR. The higher-frequency response used to couple to  $\epsilon(\omega)$  was created

by the dipole-like interaction of the metallizations in adjacent unit cells.

The magnetic response was created by combining the ERR with a cross structure Fig.1(b) in a parallel structure separated by a layer of benzocyclobutane (BCB) Fig.1(c). The magnetic component  $\mathbf{H}$  of a TEM wave coupled to the center stalks of the two metallizations that were perpendicular to the propagation vector, such that anti-parallel currents were driven. A polarization-sensitive design based on similar parameters has been shown at both THz [23] and microwave[22] frequencies.

Practical realization of metamaterials dictates the use of a support substrate that complicates the theoretical optimization of the structure. This substrate is typically thick in the propagation direction compared to the thickness of the metamaterial and the lateral unit cell dimensions. This supporting structure introduces ambiguity in the definition of the unit cell as well as significant asymmetry in the propagation direction, both of which complicate the definition of  $Z_{eff}$  and  $n_{eff}$ . [30] However, some portion of the substrate must be included in simulation because it has a measurable effect on the form of the MM resonances due to the dielectric of the substrate,  $\epsilon_s$  [31].

The effect of the substrate on the MM's resonances can be shown directly in simulation. A parameter sweep of the substrate thickness  $d$  shows that the effect of the added dielectric on the MM resonance saturates near a value of  $d = d_s$ . For  $d > d_s$ , the only added effect is a factor  $\exp(i\sqrt{\epsilon_s}k(\omega)(d - d_s))$  to  $\tilde{t}(\omega)$ . As substrates are typically chosen for low loss in the frequency range of interest,  $|\tilde{t}(\omega)|$  is virtually unchanged and the extended substrate only adds phase. The appropriate unit cell boundary in the propagation direction is therefore given by  $d_s$  and the MM elements on the substrate. The impedance mismatch at the MM-substrate and substrate-air boundaries can then be incorporated into the homogenized effective medium as these boundaries are within the unit cell.

The extracted optical constants for the metamaterial absorber shown in Fig. 1 are plotted in Fig. 2. The real and imaginary components  $\tilde{\epsilon}$  and  $\tilde{\mu}$ , as plotted in Fig. 2 (a),(c), are complicated by the effects of spatial dispersion, as previously mentioned. However, various features of the plots enable interpretation of the forms of these curves. The lowest frequency feature in  $\epsilon_2$  at  $\omega = 800$  GHz, shown in Fig. 3(c), is the conventional MM ELC resonance. Notice this is accompanied by an antiresonance in  $\tilde{\mu}(\omega)$ , which is characterized by a negative imaginary component that peaks at the center frequency of  $\epsilon_1(\omega)$ , defined by the cusp near  $\omega = 1.02$  THz, and in accord with previous work[26]. A second electric resonance appears at approximately  $\omega = 1.125$  THz due to the cut-wire response of the cross. This is accompanied by an antiresonance in  $\tilde{\mu}(\omega)$  centered at the same frequency. The resonance in  $\tilde{\mu}(\omega)$  is weak relative to the neighboring resonances in  $\epsilon$ , and thus difficult to observe.

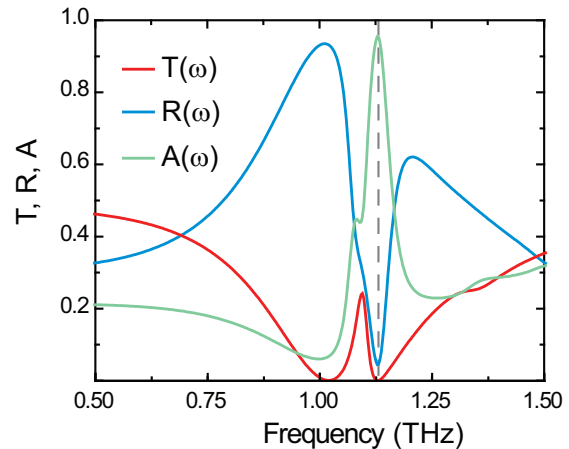


FIG. 2: (color) Reflectance (blue), Transmission (red), and Absorptivity (green) for the simulated absorber. The vertical dashed line indicates the frequency of maximum absorptivity.

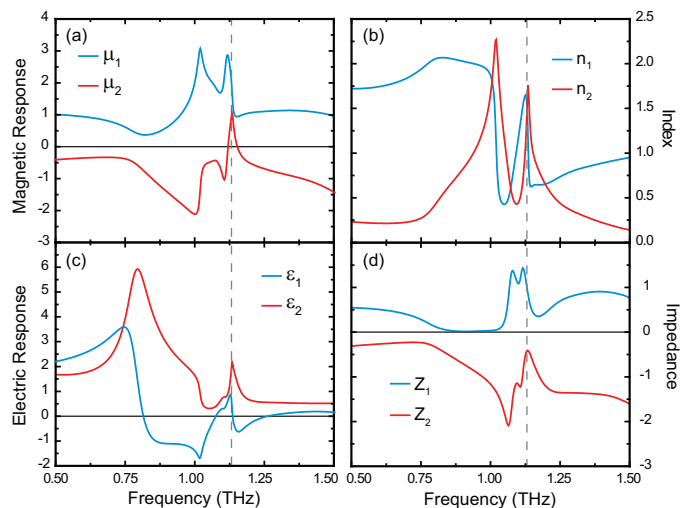


FIG. 3: (color) Real (blue) and imaginary (red) components of  $\epsilon$  and  $\mu$ . Real (blue) and imaginary (red) components of  $n$  and  $Z$ . The vertical dashed line indicates the frequency of maximum absorptivity.

However,  $\mu_2$  has a distinct positive peak at 1.13 THz. This, combined with an approximately Pendrian curve in  $\mu_1$ , indicates the presence of a magnetic response centered at this frequency. There is also a small but distinct kink in  $\tilde{\epsilon}(\omega)$  due to the antiresonance caused by the magnetic response.

Figure 2(b) shows the refractive index  $\tilde{n}(\omega)$  and (d) impedance  $\tilde{Z}(\omega)$  and demonstrates how close the structure approximates an ideal absorber. At 1.13 THz the real impedance is near unity,  $Z_1 \sim 1$ , and the complex impedance  $Z_2$  is minimized, such that  $R \sim 0$ . As desired, the imaginary index,  $n_2$ , is maximized near a value of

$\sim 1.75$ , which minimizes  $T$ . This results in a peak absorptivity of 95%, plotted as the green solid curve shown in Fig. 2.

## FABRICATION & EXPERIMENT

The two layer metallization MM absorber sample was fabricated on a high resistivity 1 mm thick silicon substrate. A 3  $\mu\text{m}$  thick SiO<sub>2</sub> layer was deposited on the Si substrate using plasma enhanced chemical vapor deposition (PECVD). The bottom, cross-shaped metallization (30 nm Ti/40 nm Pt/200 nm Au) was patterned using standard negative lithography, metal evaporation, and metal lift-off. The BCB dielectric (Cyclotene 3022-46, Dow) was deposited using two consecutive spin-coat depositions and soft cures in a vacuum oven, resulting in a final thickness of approximately six microns. The top ELC metallization layer structure and patterning used the same process as that of the cross. The two unit cells (one for each layer) are shown as the insets to the bottom panel of Fig. 4.

The MM absorber sample was examined experimentally using a Fourier Transform Infrared (FTIR) spectrometer. Polarized light from a mercury arc-lamp was transmitted and reflected from both the sample and a reference substrate, and then focused on the detector, a liquid helium cooled Si-bolometer. Measurements of the sample for both polarizations were characterized and we found no deviations within experimental error. Measured  $T(\omega)$  and  $R(\omega)$  were used to calculate the experimental  $A(\omega)$ .

Fabrication tolerances in the structures resulted in some deviation from the theoretically optimized case, and are shown in Figure 4. The corners of the ELC and cross structures are slightly rounded, and the BCB thickness was 6  $\mu\text{m}$  rather than the optimal 5.8  $\mu\text{m}$ . All of these factors were incorporated into the computer model and the re-simulated transmission, reflection, and absorption for the metamaterial absorber are shown in Figure 4, with the experimental measurement of  $T(\omega)$  and  $R(\omega)$ . In comparison to the theoretically optimized structure results shown in Figure 2, the fabricated sample exhibits a shift in the MM resonances. The first transmissive minimum has shifted by 10GHz, while the second minimum has shifted by 54GHz, both to higher frequencies. The minimum in reflectance has shifted from 1.128 THz to 1.15 THz. This is expected as electric responses are sensitive to metallic structure rounding [21] and the thickness of the BCB layer partially determines the magnetic coupling. However, this change in geometrical parameters does not fully account for the disagreement between Figures 2 and 4.

At 0.5 THz,  $T(\omega)$  and  $R(\omega)$  are well matched in experiment and simulation, but the forms deviate as the curves approach the MM resonances. Specifically, the

experimental reflectivity reaches a minimum of only 18% compared to the simulated value of 2%. Likewise, the first and second transmissive minima reach values of 3% and 3%, respectively, as opposed to less than 0.1% in simulation. Several mechanisms may be behind this disparity.

The off-resonant agreement indicates that the discrepancies are related to resonant forms of the constitutive parameters  $\tilde{\epsilon}$  and  $\tilde{\mu}$ . As indicated by Eq. 7 lowering  $F$  or increasing  $\gamma$  of the resonances translates into a higher minimum in  $T(\omega)$  as the peak value of the effective loss ( $n_2$ ) is decreased. This also changes the form of  $\tilde{Z}(\omega)$ , and therefore the form of  $R(\omega)$ .

For both the electric and magnetic resonances,  $\gamma$  is primarily determined by the loss in the BCB substrate between the ELC and cross. Previous work has determined that dielectric losses are the primary mechanism, and may be an order of magnitude greater than Ohmic loss[22]. Also, because BCB is the primary dielectric that tunes the capacitance of each structure, any deviation from the nominal value of  $\epsilon = 2.5$  will lead to variation in absorbance. Further, it is well known that the dielectric value of many polymer compound have significant dependence on frequency, especially within the THz range[32]. As previously mentioned, the “strength of the oscillator”  $F$  is determined by the geometry, filling fraction, and conductivity of the two metallizations. Therefore, the deviation of experimental curves in Fig. 4 may be caused by a combination of increased loss in the BCB and lowered conductivity in the metallizations.

The best fit of simulation to experimental data is shown in Figures 4 and 5. The loss tangent of BCB was found to be approximately one order of magnitude greater than the nominal value, while the conductivity of gold was found to have decreased an order of magnitude. As a consequence of the non-uniform shift of both the magnetic and electric resonances, as well as increased damping due to loss,  $\tilde{n}$  and  $\tilde{Z}$  have deviated from their optimum values, resulting in a peak absorptivity of 74% (Fig. 5).

## DISCUSSION

We now discuss the potential use of the metamaterial absorber as a thermal imager for the THz frequency range. Compared to existing THz absorbers, our device is narrow band. This enables spectrally-selective applications, such as in the detection of explosives. However, unlike previous MM absorber designs[23], our device is polarization insensitive. This may be ideal for certain applications, as it maximizes absorption for arbitrarily polarized or incoherent light. As a MM device, our design is geometrically scalable to different frequency ranges. This scalability is limited only by limitations in fabrication and loss in constituent materials. The limitations

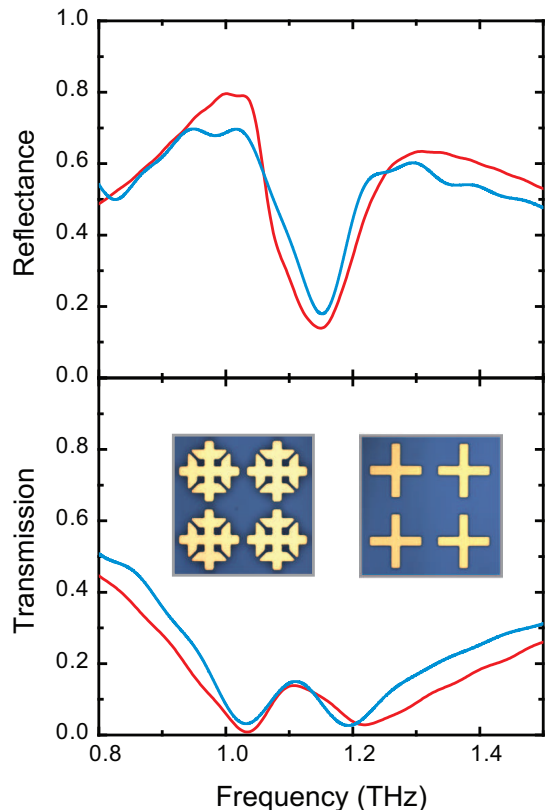


FIG. 4: (color) Reflectance and transmission results for experiment (blue) and simulation (red)

of the narrow band, resonant design could be overcome by using multiple distinct unit cells[33] or by incorporating tunable or frequency agile metamaterial components [34].

It should be noted that designs presented here are bianisotropic - a result of asymmetry in the propagation direction - and belong to Shönflies point group  $C_4$ . [35] We have performed simulations, (not shown), in order to elucidate the impact of the bianisotropy on absorptive properties of the metamaterial. We studied the cross polarization in transmission as a function of frequency for the design shown in Fig. 1. Computer simulations indicate that the cross polarization is small and achieves a maximum of only  $10^{-4}$  over the frequency range of interest. We also investigated the cross polarizations for designs presented in Refs. [22, 23] and found similar results. Thus, for normal incidence radiation, the effect of bianisotropy is negligible.

In conclusion, we have derived general conditions to create an absorber based on effective medium theory, and for the specific case of MM elements. We have shown that such a design can reach absorptivities approaching unity within a narrow band. We have also successfully implemented this approach with a THz frequency absorber

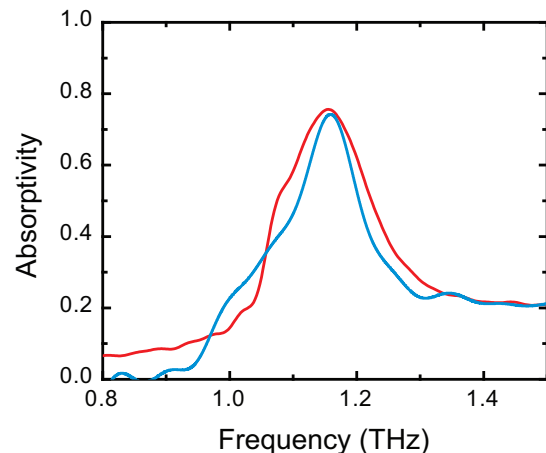


FIG. 5: (color) Experimental (blue) and simulated (red) Absorptivity curves.

design. The theory presented here and the design specifically show great promise to creating absorbers at any decade of frequency.

- 
- [1] F. Oliveira, R. Barat, B. Schulkin, F. Huang, J. Federici, and D. Gary, Proc. SPIE **5070**, 60 (2003).
  - [2] D. Zimdars, Proc. SPIE **5070**, 108 (2003).
  - [3] H.-B. Liu, Y. Chen, G. J. Bastiaans, and X.-C. Zhang, Opt. Express **11**, 2549 (2003).
  - [4] J. Barber, D. E. Hooks, D. J. Funk, R. D. Averitt, A. J. Taylor, and D. Babikov, J. Phys. Chem A **109**, 3501 (2005).
  - [5] X.-C. Zhang, Phys. Med. Biol. **47**, 3667 (2002).
  - [6] T. W. Crowe, T. Globus, D. L. Woolard, and J. L. Hessler, Philosophical Transactions of the Royal Society of London A **362**, 265 (2004).
  - [7] R. H. Jacobsen, D. M. Mittleman, and M. C. Nuss, Opt. Lett. **21**, 2011 (1996).
  - [8] D. M. Mittleman, J. Cunningham, M. C. Nuss, and M. Geva, Appl. Phys. Lett. **71**, 16 (1997).
  - [9] G. P. Williams, Rep. Prog. Phys. **69**, 301 (2006).
  - [10] M. Tonouchi, Nat. Photonics **1**, 97 (2007).
  - [11] J. B. Pendry, A. J. Holden, W. J. Stewart, and I. Youngs, Phys. Rev. Lett. **76**, 4773 (1996).
  - [12] J. B. Pendry, A. J. Holden, D. J. Robbins, and W. J. Stewart, IEEE Trans. Microwave Theory Tech. **47**, 2075 (1999).
  - [13] T. J. Yen, W. J. Padilla, N. Fang, D. C. Vier, D. R. Smith, J. B. Pendry, D. N. Basov, and X. Zhang, Science **303**, 1494 (2004).
  - [14] M. C. K. Wiltshire, J. B. Pendry, I. R. Young, D. J. Larkman, D. J. Gilderdale, and J. V. Hajnal, Science **291**, 849 (2001).
  - [15] D. R. Smith, W. J. Padilla, D. C. Vier, S. C. Nemat-Nasser, and S. Schultz, Phys. Rev. Lett. **84**, 4184 (2000).
  - [16] M. Gokkavas, K. Guven, I. Bulu, K. Aydin, R. S. Penciu, M. Kafesaki, C. M. Soukoulis, and E. Ozbay, Phys. Rev.

- B **73**, 193103 (2006).
- [17] S. Linden, C. Enkrich, M. Wegener, J. Zhou, T. Koschny, and C. M. Soukoulis, *Science* **306**, 1351 (2004).
- [18] S. Zhang, W. Fan, N. C. Panoiu, K. J. Malloy, R. M. Osgood, and S. R. J. Brueck, *Phys. Rev. Lett.* **95**, 137404 (2005).
- [19] G. Dolling, M. Wegener, C. M. Soukoulis, and S. Linden, *Opt. Lett.* **32**, 53 (2007).
- [20] J. B. Pendry, D. Schurig, and D. R. Smith, *Science* **312**, 1780 (2006).
- [21] D. Schurig, J. J. Mock, B. J. Justice, S. A. Cummer, J. B. Pendry, A. F. Starr, and D. R. Smith, *Science* **314**, 977 (2006).
- [22] N. I. Landy, S. Sajuyigbe, J. J. Mock, D. R. Smith, and W. J. Padilla, *Phys. Rev. Lett* **100**, 207402 (2008).
- [23] H. Tao, N. I. Landy, C. M. Bingham, X. Zhan, R. D. Averitt, and W. J. Padilla, *Opt. Express* **16**, 7181 (2008).
- [24] D. R. Smith, D. C. Vier, T. Koschny, and C. M. Soukoulis, *Phy. Rev. E* **71**, 036617 (2005).
- [25] A. Serdyukov, I. Semchenko, S. Tretyakov, and A. Sihvola, *Electromagnetics of Bi-anisotropic Materials: Theory and Applications* (Gordon and Breach Science Publishers, 2001).
- [26] R. Liu, T. J. Cui, D. Huang, B. Zhao, and D. R. Smith, *Phy. Rev. E* **76**, 026606 (2007).
- [27] W. J. Padilla, M. T. Aronsson, C. Highstrete, M. Lee, A. J. Taylor, and R. D. Averitt, *Physical Review B* **75**, 041102(R) (2007).
- [28] D. Schurig, J. J. Mock, and D. R. Smith, *Appl. Phys. Lett.* **88**, 041109 (2006).
- [29] D. R. Smith, J. Gollub, J. J. Mock, W. J. Padilla, and D. Schurig, *Journal of Applied Physics* **100**, 024507 (2006).
- [30] C. R. Simovski and S. A. Tretyakov, *Phys. Rev. B* **75**, 195111 (2007).
- [31] W. J. Padilla, D. R. Smith, and D. Basov, *J. Opt. Soc. Am. B.* **23**, 3 (2006).
- [32] H. Tao (2008), unpublished.
- [33] C. M. Bingham (2008), unpublished.
- [34] H.-T. Chen, J. F. O'Hara, A. K. Azad, A. J. Taylor, R. D. Averitt, D. B. Shrekenhamer, and W. J. Padilla, *Nature Photonics* **2**, 295 (2008).
- [35] W. J. Padilla, *Opt. Exp.* **15**, 1639 (2007).